Insight into the Self-Assembly Behaviors of Per- and Polyfluoroalkyl Substances Using a "Computational Microscope"

Bei Yan [a, b*], Riccardo Alessandri [c,d], Siewert J. Marrink [e], Linda S. Lee [b], Jinxia Liu [a,f*]

[a] Department of Civil Engineering, McGill University, 817 Sherbrooke Street West, Montreal, Quebec H3A 0C3, Canada

[b] Department of Agronomy, Environmental & Ecological Engineering, Purdue University, 615 Mitch Daniels Blvd., West Lafayette, IN 47907-2053 USA

[c] Pritzker School of Molecular Engineering, University of Chicago, Chicago, IL, 60637, USA

[d] Department of Chemical Engineering, KU Leuven, Celestijnenlaan 200J, 3001 Leuven, Belgium

[e] Groningen Biomolecular Sciences and Biotechnology Institute, University of Groningen, Nijenborgh 7, 9747 AG Groningen, the Netherlands

[f] Department of Civil and Environmental Engineering, Hong Kong Polytechnic University, Kowloon, Hong Kong SAR China

[*]Corresponding authors: jinxia.liu@mcgill.ca; yan519@purdue.edu
The majority of the work was carried out during the corresponding authors' time at McGill University.

Abstract:

Aqueous film-forming foams (AFFF) have been extensively used for firefighting, contributing to environmental contamination with per- and polyfluoroalkyl substances (PFAS). Most PFAS in AFFFs are fluorosurfactants, known to self-assemble into large supramolecular assemblies in the field of physical chemistry; however, application of this phenomenon to understanding environmental fate has not been studied. We hypothesize that self-assembled PFAS likely enhances the long-term retention of PFAS in subsurface environments, acting as a continuous source of dissolved PFAS. Thus, characterizing these self-assemblies and understanding their aggregation dynamics are crucial for assessing PFAS fate and transport. Despite the utility of molecular dynamics (MD) simulation in studying surfactant behaviors, fluorosurfactants have been underexplored due to the lack of force field parameters. In this study, we developed coarse-grained (CG) force field parameters for fluorosurfactants based on the Martini 3 model and performed CG-MD simulations. These "computational microscope" simulations reveal the self-assembly behaviour of selected PFAS, aligning with experimental cryo-TEM observations and providing mechanistic insights. Our work sheds light on the evolution of solvated PFAS self-assemblies over time and space. The CG-MD simulation can particularly address the knowledge gaps for new PFAS that are difficult to explore experimentally due to the lack of chemical standards.

Keywords: PFAS; Self-assembly; Vesicle; Coarse-grained molecular dynamics simulation; cryo-TEM.

Synopsis: A novel coarse-grain MD simulation approach was developed to study the self-assembly behaviours of PFAS, revealing their unique environmental behaviour.

45 **Graphic for manuscript:**

46 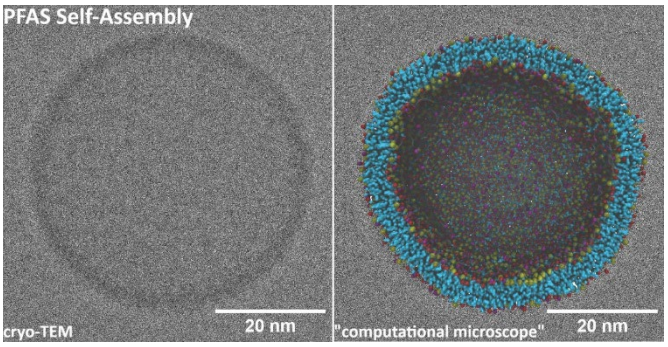

47

48

Introduction

Aqueous film-forming foams (AFFF) historically used for fighting Class B fires contain per- and polyfluoroalkyl substances (PFAS), primarily fluorosurfactants, which have high heat resistance and help spread the foam and create a thin film of water for cooling and suppressing the fire.[1, 2] Globally, many fire training areas, military bases, oil refineries, and airports have been negatively impacted by residual PFAS from AFFF usage.[3-5] Despite cessation of AFFF use, PFAS persist in subsurface environments, such as soils and aquifers, with concentrations remaining high decades later. [3, 6] For example, the summed concentration of 15 PFAS in groundwater near an Air Force Base, though no longer in operation since 1993, was determined to be 64.9 μg/L in 2021,[7] more than one million times higher than the drinking water health advisor levels set by U.S. EPA.[8] Current knowledge based on hydrocarbon surfactants fails to explain this persistence, highlighting the need for new insights into PFAS behavior.

Physical chemistry literature suggests that perfluoroalkyl chains' strong hydrophobicity and weak van der Waals interactions facilitate the self-assembly of fluorosurfactants into stable supramolecular structures in water and at interfaces.[9] If such assemblies do occur in AFFF-impacted sites, they could serve as a long-term source of dissolved PFAS. However, characterizing these structures in AFFF-impacted natural and engineered systems (e.g., soils, groundwater aquifers, and filtration facilities using activated carbon or ion exchange resins) remains challenging, making their role in PFAS transport and fate hypothetical. Understanding PFAS self-assembly is crucial, for instance, if PFAS truly self-assemble at interfaces, new transport models need to consider such unique aggregation to enable better prediction of their environmental behaviors.

Advanced techniques like cryo-transmission electron microscopy (cryo-TEM) and solid-state NMR can provide insights into supramolecular architectures, but they fall short in detailing the

mechanisms of formation, composition, structure, and phase transitions.[10, 11] *In silico* simulations such as molecular dynamics (MD), in principle, can fill this gap by offering atomic-resolution details of interactions within the system.[10, 12-14] MD simulations come in two main forms: all-atom and coarse-grained (CG) MD simulations. All-atom models consider force field (FF) parameters for every atom in a system and offer the highest level of resolution for classical MD simulations, excluding quantum-based approaches. However, they are currently limited to small-scale (in both time and length regimes) aggregation processes such as formations of micelles, hemi-micelles,[15] and bilayers.[16]

CG models, which represent groups of atoms as CG beads while retaining their chemical specificity, extend the spatiotemporal range of MD simulations (from nanometers to micrometer and nanosecond to millisecond). CG-MD simulation has been an indispensable tool to complement experimental techniques for gaining insights into lipid or surfactant based processes such as transformation between phases, membrane domain formation, and spontaneous self-assembly into vesicles.[10, 17] To date, only a limited number of CG-MD simulation studies of PFAS have been reported, e.g., the cylindrical-like aggregation and random coil conformations of perfluorosulfonic acid polymer in water-ethanol mixture,[14, 18] despite the paramount importance of this class of compounds.

In this paper, we developed CG models of PFAS molecules (as displayed in Figure 1) based on the popular Martini 3 model[19, 20] and performed MD simulations to predict their aggregation states in water. We considered pure systems of perfluorooctanoic acid (PFOA), perfluorooctane sulfonate (PFOS), 6:2 fluorotelomer sulfonic acid (6:2 FtSA), and perfluorooctaneamido ammonium iodide (PFOAAmSI), as well as binary PFOA+PFOS systems. These PFAS were chosen due to their environmental prevalence and regulatory significance.[21, 22] In the results section,

we first cover the self-assembly process of a single PFAS species, and then describe in more detail the vesicle structure formed by PFOA and PFOS. Cryo-TEM was employed to validate the self-assembled PFAS structures in the binary system predicted by the simulations. Our study demonstrated the availability and utility of a novel tool to study PFAS behaviors in new ways previously impossible.

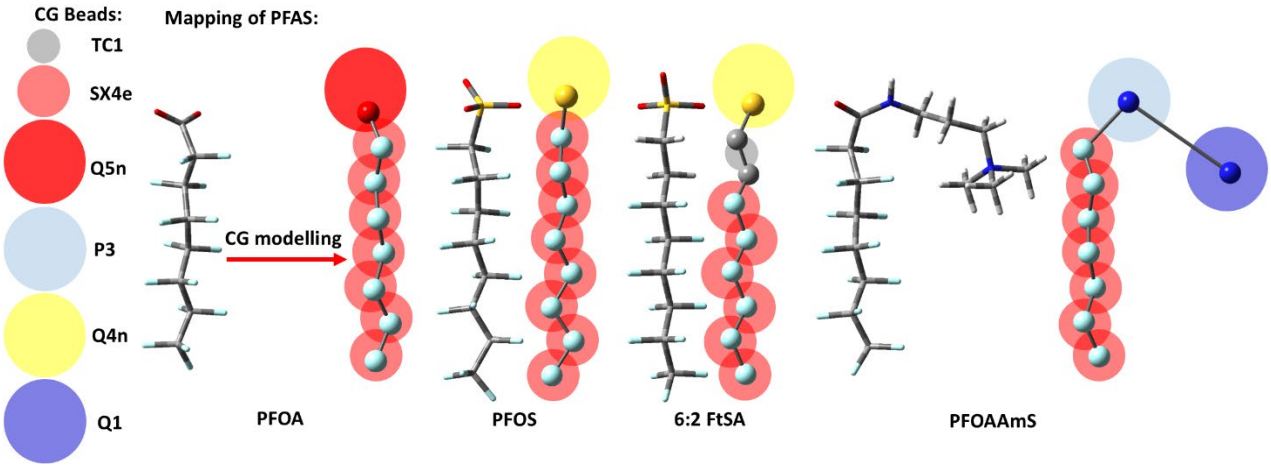

Figure 1. Structure and nomenclature of PFOA ($CF_3(CF_2)_6COO^-$), PFOS ($CF_3(CF_2)_7SO_3^-$), 6:2 FtSA ($CF_3(CF_2)_5(CH_2)_2SO_3^-$), and PFOAAmS ($CF_3(CF_2)_6CONH(CH_2)_3N^+(CH_3)_3$) in the coarse-grained model. In the tube representation of PFAS molecules: gray, C atom; light gray tube, H atom; red tube, O atom; navy blue tube, N atom; cyan-blue tube, F atom; yellow tube, S atom.

Materials and Methods

CG Modeling of PFAS Based on the Martini 3 Force Field

CG models of PFAS (Figure 1) were built following the Martini 3 method for small molecules.[20] However, we found that the default bead type for the CF_2 group required optimization, due to the large van der Waals diameter and extremely hydrophobic nature of this group.[23] To capture these trends, the bead size and Lennard-Jones (LJ) potential for F-alkyl chains interactions were optimized to (i) obtain a stiff PFAS chain that (ii) self-assembles into lamellar structures, as

detailed in Table S1 and the Supporting Information (SI). Based on this model, we performed MD simulations from randomly oriented PFAS in water (Table S2), using the GROMACS 2023.3 package.[24, 25] These parameters were validated by aligning the simulation results with experimental data: 1) with cryo-TEM images (e.g., morphology, structure, and size) and 2) with the reported diffusion coefficients of PFAS.[26]

Results and Discussion

Spontaneous Self-Assembly of Single-Chain PFAS

We started with performing CG-MD simulations on four PFAS species in water individually to visualize self-assembly from monomers to micelles and vesicles. Each system consisted of 1516 molecules (e.g., anionic surfactants PFOA, PFOS, 6:2 FtSA, or the cationic PFOAAmS; and neutralized by either K^+ or I^-), initially placed randomly in a 29×29×29 nm^3 simulation box (Systems Random I-IV, Table S2). Figure 2 illustrates the PFOA aggregation process: the initially dispersed PFOA surfactants spontaneously cluster into micelles within 16 ns (Figure 2b) and coalesce almost immediately to form threadlike/wormlike structures shown in Figure 2c (t = 40 ns). These irregular structures grow and transform themself into several bilayer structures (Figure 2d, t = 200 ns) and merge into a single bilayer with curved edges (Figure 2e, t = 1.2 μs, length of the bilayer ~ 25 nm, and Figure 2f, t = 1.36 μs). The curved edges give rise to a large line tension due to the solvent (water) exposure. The large line tension is subsequently minimized by gradually encapsulating solvent water (with counterions as well), leading to a cuplike structure containing a small pore (Figure 2g, t = 1.4 μs). Eventually, the pore was disrupted at t = 1.6 μs, resulting in a unilamellar vesicle (diameter 15.4 nm) with a water core illustrated in Figure 2h. This pathway resembles that of double-chain amphiphiles such as dipalmitoylphosphatidylcholine.[27] However, the formation of vesicles by a single chain PFAS is noteworthy, despite being observed in various

systems,[28] indicating the unique properties conferred by fluorine in PFAS. The vesicle remained stable over a 10 μs simulation, evidenced by the root mean square deviation (RMSD) analysis (Figure S1).

The vesicle formation of PFOS, 6:2 FtSA, and PFOAAmS followed the same aggregation pathway to PFOA, i.e., random orientation of PFAS in water → micelles and threads/worms→bilayers→cuplike vesicle→unilamellar vesicle (see Figure S2-S7). Complete vesicles always formed within 2 μs and remained stable during over the 10 μs simulation times with low RMSD values. For 6:2 FtSA, beside the vesicle, some molecules formed a separate bilayer (Figure S4). PFOAAmS cations formed a small vesicle within 600 ns, which then merged with nearby bilayers to form a larger vesicle (Figure S7). The cryo-TEM images of PFOA (Figure S8) and PFOAAmS (Figure S9) confirmed the vesicle formation in anionic and cationic PFAS solutions. Dynamic light scattering (DLS) of PFOA (Figure S10) and PFOS (Figure S11) showed particle size distributions consistent with reported micelle and vesicle (30-300 nm, imaged by cryo-TEM) formed by fluorosurfactants.[28, 29]

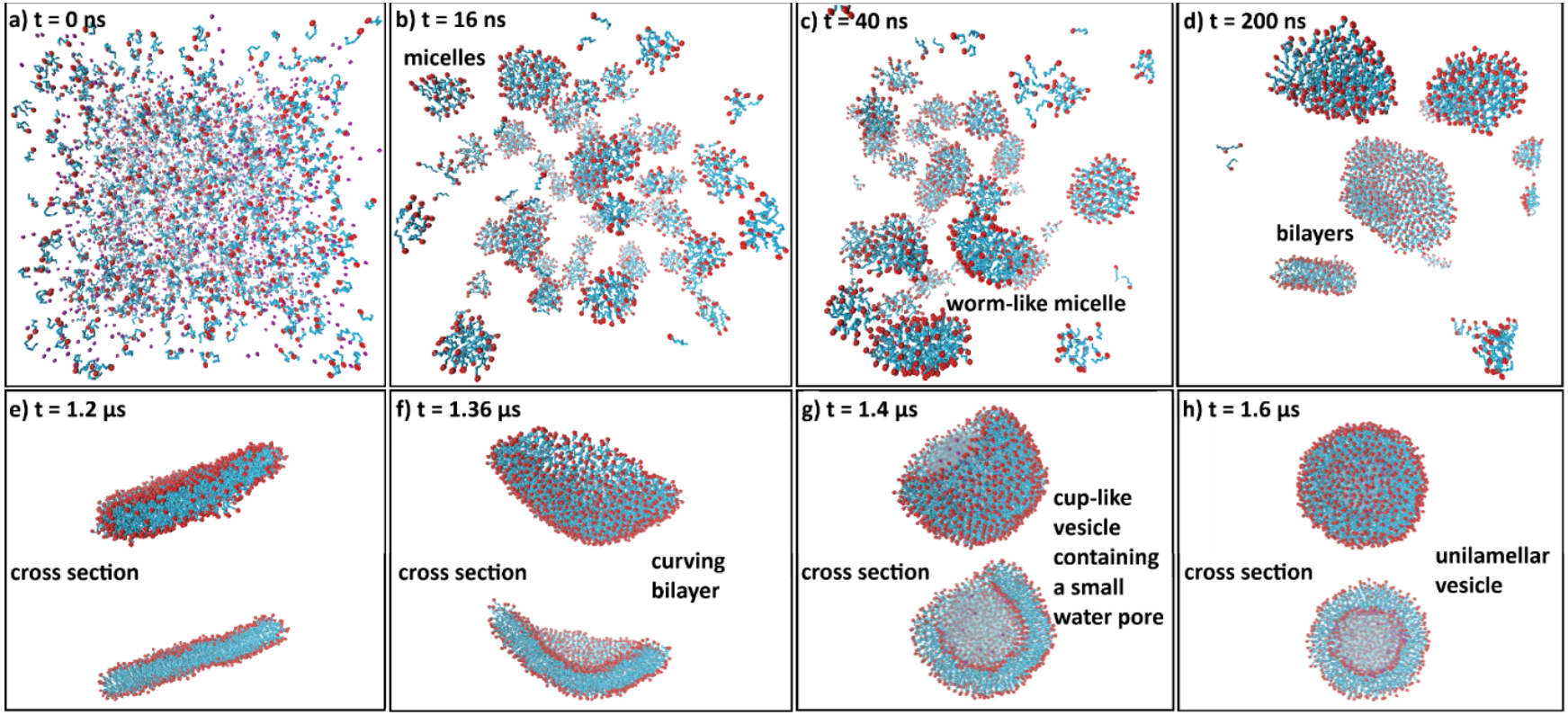

Figure 2. Aggregation process of PFOA anions from a random solution (1516 PFOA in a 29×29×29 nm^3 simulation box) into a vesicle. Cyan-blue and red represent the hydrophobic CF chain and carboxylate group, respectively; purple balls are potassium ions to neutralize the system. For clarity, water and counter ion (K^+) are not shown (except for K^+ at t = 0 ns). Snapshots are shown at t = 0 ns (a), 16 ns (b), 40 ns (c), 200 ns (d), 1.2 µs (e), 1.36 µs (f), 1.4 µs (g), 1.6 µs (h), see text for detailed description of the vesicle formation. The root mean square deviation (RMSD) of PFOA in the vesicle in the last 200 ns off to 0.18 nm (Figure S1), indicating the vesicle structure is quite stable.

Structure of Self-Assembled PFAS

Because PFAS are mostly present as mixtures in the environment,[7, 22] this raises the question of how coexisting PFAS species form supramolecular aggregates. To investigate this, we simulated a binary system containing 758 PFOA and 586 PFOS in a 65×65×65 nm^3 box, equivalent to 2 mg/mL PFOA + 2 mg/mL PFOS in water (System Random V, Table S2) and in the range of reported CMC values of PFAS.[30, 31] A stable vesicle with a 17.8 nm diameter formed after 30 μs simulation (displayed in Figure 3a, RMSD in Figure S12). There are 209 PFOA and 213 PFOS in the inner shell and 549 PFOA and 373 PFOS in the outer shell. It appears that PFOA is strongly enriched in the outer monolayer, presumably because of the more hydrophilic head and shorter tail, resulting in an effective positive curvature preference compatible with the outer monolayer.[32-34]

The vesicle structure was further characterized by the radial distribution function (RDF) $g(r)$ of the terminal -CF_3, CF chain, carboxylate group of PFOA, sulfonate group of PFOS, counter ion K^+, and water from the center-of-mass of the vesicle (Figure 3b). The vesicle shell consists of two layers of PFOA + PFOS, with an extremely hydrophobic interior of the perfluoroalkyl chain and a hydrophilic exterior of the carboxylate and sulfonate groups. The lamellar shell thickness is ~3.2 nm, measured from the peaks of sulfonate distributions. The RDFs are asymmetric, showing differences between the inner and outer monolayers. The sulfonate headgroup has a higher peak in the inner monolayer, likely due to greater water penetration in the outer layer.[27] This trend is mirrored by the counterion K^+. The perfluoroalkyl tail region also shows more subtle differences; the density of the outer monolayer is higher than that of the inner monolayer, which is opposite to the headgroups. These effects may result from the curved nature of the lamellar layer, causing a cone-shaped volume available for PFAS molecules in the outer leaflet, with relatively more space for the headgroup and less for the tail - in the inner leaflet this is reversed.

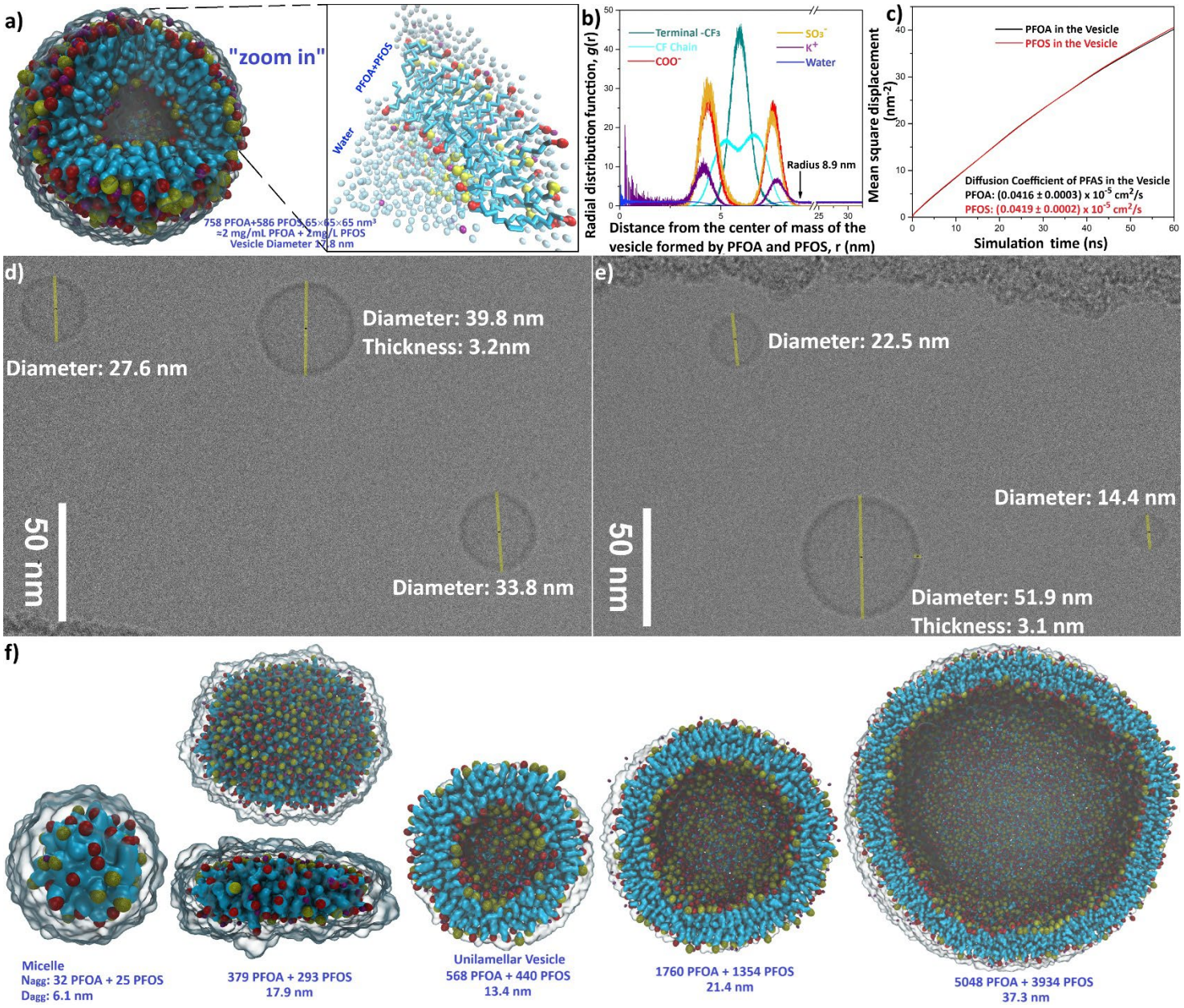
a)
"zoom in"
PFOA+PFOS
Water
758 PFOA+586 PFOS 65×65×65 nm³
≈2 mg/mL PFOA + 2mg/L PFOS
Vesicle Diameter 37.8 nm
b)
Terminal -CF₃
CF Chain
COO⁻
SO₃⁻
K⁺
Water
Radius 8.9 nm
Radial distribution function, g(r)
Distance from the center of mass of the vesicle formed by PFOA and PFOS, r (nm)
c)
PFOA in the Vesicle
PFOS in the Vesicle
Mean square displacement (nm⁻²)
Diffusion Coefficient of PFAS in the Vesicle
PFOA: (0.0416 ± 0.0003) x 10⁻⁵ cm²/s
PFOS: (0.0419 ± 0.0002) x 10⁻⁵ cm²/s
Simulation time (ns)
d)
Diameter: 27.6 nm
Diameter: 39.8 nm
Thickness: 3.2nm
50 nm
Diameter: 33.8 nm
e)
Diameter: 22.5 nm
Diameter: 14.4 nm
50 nm
Diameter: 51.9 nm
Thickness: 3.1 nm
f)
Micelle
Nagg: 32 PFOA + 25 PFOS
Dagg: 6.1 nm
379 PFOA + 293 PFOS
17.9 nm
Unilamellar Vesicle
568 PFOA + 440 PFOS
13.4 nm
1760 PFOA + 1354 PFOS
21.4 nm
5048 PFOA + 3934 PFOS
37.3 nm

178

Figure 3. Self-assembled structures spontaneously formed from PFOA and PFOS monomers. a) a cross-section view of a vesicle formed by 758 PFOA and 586 PFOS at 40 μs CG molecular dynamics simulation in a 65×65×65 nm^3 simulation box (equivalent to 2 mg/mL of PFOA and 2 mg/mL of PFOS). Cyan-blue, red, yellow represent the hydrophobic CF chain, carboxylate group, sulfonate groups, respectively; purple balls are potassium ions, and ice blue represents the solvent (water). For clarity, the water bulk phase and the counter ions K^+ in the water bulk phase were not shown; b) radial density function *g*(r) of the terminal -CF_3 group, CF chain (6 ~ 7 SX4e beads), head groups (carboxylate group Q5n bead, and sulfonate group Q4n bead), the counter-ion (potassium ion), and solvent water as a function of distance from the vesicle center obtained in the last 400 ns; c) mean square displacement (MSD) of PFOA and PFOS in the vesicle and the determined diffusion coefficients (fitting to the slope of the MSD over the 60 ns simulation); d) and e) cryo-TEM images of vesicles formed by PFOA (2 mg/mL) and PFOS (2 mg/mL), lower magnification images and DLS analysis were provided in SI (Figure S14-S16); f) simulation-generated morphologies of assemblies for increasing the number of monomers (N_{agg}). Each subsequent image shows the cross-section through the middle of the supramolecular aggregate once it has stabilized after self-assembly.

Although the vesicles formed by PFAS appear stable, the individual molecules are still capable of diffusing, indicating a two-dimensional fluid-like state. To quantify this mobility, we computed the mean square displacement (MSD) of PFAS molecules. Fitting the slope of MSD gives access to the lateral diffusion constant (Figure. 3c). The diffusion coefficients of PFOA and PFOS in vesicle were both $(0.042 \pm 0.001) \times 10^{-5}$ cm^2/s, similar to typical phospholipids in vesicles but much slower than the diffusion of these lipids in the aqueous phase. Single-molecule simulations (Systems Random XI, XII) yielded diffusion rates of $(0.626 \pm 0.004) \times 10^{-5}$ cm^2/s for PFOA and $(1.013 \pm 0.003) \times 10^{-5}$ cm^2/s for PFOS (Figure S13), comparable to experimental values for PFOA (0.437×10^{-5} cm^2/s) and PFOS (0.508×10^{-5} cm^2/s)[26] and over 15 times faster than those in the vesicular membrane.

As an initial validation of the simulation results, cryo-TEM on the 1:1 PFOS:PFOA mixture was conducted. Vesicles with various diameters, such as 11.4, 22.5, 33.8, and 51.9 nm, were recorded by cryo-TEM (Figures 3d and 3e). The thickness of the layers was measured to be 3.1 to 3.2 nm, which is highly consistent with the measured results from the sulfonate peaks of RDF. The cryo-TEM images of vesicular structures of PFOA and PFOS in a binary mixture provides evidence of self-assembly, confirming the results from our simulations.

To simulate a broader range of vesicle sizes observed in cryo-TEM images, we performed simulations of PFOA+PFOS binary systems with increasing aggregation number, N_{agg} (Systems Random V-X, Table S2). These simulations revealed stable supramolecular structures (Figure 3f), ranging from small micelles (N_{agg}=55) to bilayer patches (N_{agg}=672) and larger unilamellar vesicles (N_{agg}>1000), aligning with the vesicles imaged by cryo-TEM. The CG-MD results indicate that there is a minimum number of PFAS monomers (~ 568 PFOA + 440 PFOS) needed to form a vesicle. Below this number, the monomers form a small bilayer patch (bicelle) that represents an early stage of the formation of a vesicle. In addition, we also carried out a CG-MD simulation at a diluted concentration (Random XIII, 8 PFOA and 6 PFOS in a 65×65×65 nm^3 simulation box, equivalent to 20 ppm of PFOA and 20 ppm of PFOS), an oligomer with 4 PFOS and 3 PFOA was observed at 10 μs (Figure S17), which is consistent with López-Fontán's study.[30]

Taken together, these findings demonstrate that our CG model is capable of predicting and reproducing the structural features of PFAS supramolecular aggregates, in particular, the ability to form stable vesicular structures in line with the experimental data.

Environmental Significance

Hydrocarbon surfactant aggregation, or the formation of micelles, typically occur at concentrations near or exceeding their critical micelle concentration. In contrast, fluorosurfactants exhibit different aggregation behaviours; they can form small aggregates at low concentrations (e.g., at picomolar concentrations)[30] and supramolecular assemblies at high concentrations. However, the implications of these behaviors for understanding AFFF-derived PFAS have not been adequately studied, primarily due to the challenges associated with observing and modeling their behaviours under environmentally relevant conditions. In AFFF-impacted environments, relevant concentrations can vary widely, ranging from high parts-per-million (ppm) to parts-per-trillion (ppt) levels. For instance, PFAS released during firefighting training or accidental discharges often start at high ppm levels (e.g., AFFFs are discharged at 1%~6% concentrates), which suggests the possibility that PFAS are, in fact, released in self-assembled forms into the environment in many cases. In addition, in engineered treatment systems, such as filtration beds filled with activated carbon, ion exchange resins or other sorbent materials, PFAS can accumulate to high concentrations from diluted contaminated water, potentially leading to aggregation on adsorbent surfaces. For instance, Zaggia et al.[35] found the adsorption capacity of ion exchange resin for certain PFAS species exceeds the anion exchange capacity of the resin several times, suggesting other mechanisms at play.

With the advent of the Martini 3.0 model and FF parameters for PFAS developed in this study, we are now equipped with a powerful new tool to simulate the possible self-assembly behaviour of PFAS, complementing experimental observations and assisting in the development of new mechanisms. Furthermore, considering the general lack of pure chemical standards for many PFAS, such as cationic and zwitterionic PFAS that are commonly found in contaminated soil and water,

these FF parameters and their application in CG-MD simulation can bridge important knowledge gaps that cannot be addressed experimentally. We invite the research community to explore further the applicability of our CG-MD simulation approach for environmentally relevant conditions for PFAS self-assembly, e.g., PFAS source zones with and without co-contaminants, surfaces of adsorbents, air-water interface, water-soil interface, etc. Note that applications involving other molecules would require further calibration of the F-alkyl bead interactions, as only a limited subset of the Martini 3 bead types was considered here. We also encourage exploration of the limitations or the artifacts of this simulation approach. Currently, the system that can be modelled still requires a relatively high PFAS concentration, but with the ever-increasing computational power available, we anticipate that modelling various environmentally relevant conditions will soon be within reach.

Appendix A. Supplementary data

The details of sample preparations, cryo-TEM, CG models, force field parameters, and computations are given in the Support Information section.

Acknowledgments

This project is supported by NSERC Discovery Grant. The MD simulations were performed on the Béluga supercomputer of Compute Canada. We want to thank members of the Facility for Electron Microscopy Research (Dr. Corbin Black, Dr. David Liu, Dr. Kaustuv Basu, and Dr. S. Kelly Sears) at McGill University for their cryo-TEM support.

References:

(1) Liu, M.; Glover, C. M.; Munoz, G.; Duy, S. V.; Sauvé, S.; Liu, J. Hunting the missing fluorine in aqueous film-forming foams containing per- and polyfluoroalkyl substances. *J. Hazard. Mater.* **2024**, *464*, 133006. DOI: 10.1016/j.jhazmat.2023.133006.

(2) Wang, Z.; DeWitt, J. C.; Higgins, C. P.; Cousins, I. T. A never-ending story of per- and polyfluoroalkyl substances (PFASs)? *Environ. Sci. Technol.* **2017**, *51* (5), 2508-2518. DOI: 10.1021/acs.est.6b04806.

(3) Adamson, D. T.; Nickerson, A.; Kulkarni, P. R.; Higgins, C. P.; Popovic, J.; Field, J.; Rodowa, A.; Newell, C.; DeBlanc, P.; Kornuc, J. J. Mass-based, field-scale demonstration of pfas retention within afff-associated source areas. *Environ. Sci. Technol.* **2020**, *54* (24), 15768-15777. DOI: 10.1021/acs.est.0c04472.

(4) Liu, M.; Munoz, G.; Vo Duy, S.; Sauvé, S.; Liu, J. Per- and polyfluoroalkyl substances in contaminated soil and groundwater at airports: A canadian case study. *Environ. Sci. Technol.* **2022**, *56* (2), 885-895. DOI: 10.1021/acs.est.1c04798.

(5) Høisæter, Å.; Pfaff, A.; Breedveld, G. D. Leaching and transport of pfas from aqueous film-forming foam (AFFF) in the unsaturated soil at a firefighting training facility under cold climatic conditions. *J. Contam. Hydrol.* **2019**, *222*, 112-122. DOI: 10.1016/j.jconhyd.2019.02.010.

(6) Awad, E.; Zhang, X.; Bhavsar, S. P.; Petro, S.; Crozier, P. W.; Reiner, E. J.; Fletcher, R.; Tittlemier, S. A.; Braekevelt, E. Long-term environmental fate of perfluorinated compounds after accidental release at toronto airport. *Environ. Sci. Technol.* **2011**, *45* (19), 8081-8089. DOI: 10.1021/es2001985.

(7) Yan, B.; Munoz, G.; Sauve, S.; Liu, J. Molecular mechanisms of per- and polyfluoroalkyl substances on a modified clay: A combined experimental and molecular simulation study. *Water Res.* **2020**, *184*, 116166. DOI: 10.1016/j.watres.2020.116166.

(8) U. S., EPA. Drinking water health advisories for PFAS fact sheet for communities. **2022**. https://www.epa.gov/system/files/documents/2022-06/technical-factsheet-four-PFAS.pdf (accessed on November 1, 2024).

(9) Krafft, M. P.; Riess, J. G. Selected physicochemical aspects of poly- and perfluoroalkylated substances relevant to performance, environment and sustainability—part one. *Chemosphere* **2015**, *129*, 4-19. DOI: 10.1016/j.chemosphere.2014.08.039.

(10) Marrink, S. J.; Corradi, V.; Souza, P. C. T.; Ingólfsson, H. I.; Tieleman, D. P.; Sansom, M. S. P. Computational modeling of realistic cell membranes. *Chem. Rev.* **2019**, *119* (9), 6184-6226. DOI: 10.1021/acs.chemrev.8b00460.

(11) Elbaum, M.; Seifer, S.; Houben, L.; Wolf, S. G.; Rez, P. Toward compositional contrast by cryo-stem. *Acc. Chem. Res.* **2021**, *54* (19), 3621-3631. DOI: 10.1021/acs.accounts.1c00279.

(12) Yan, B.; Wang, J.; Liu, J. Stxm-xanes and computational investigations of adsorption of per- and polyfluoroalkyl substances on modified clay. *Water Res.* **2021**, *201*, 117371. DOI: 10.1016/j.watres.2021.117371.

(13) Yan, B.; Liu, J. Molecular framework for designing fluoroclay with enhanced affinity for per- and polyfluoroalkyl substances. *Water Res. X* **2023**, *19*, 100175. DOI: 10.1016/j.wroa.2023.100175.

(14) Minervino, A.; Belfield, K. D. Review of recent computational research on the adsorption of PFASs with a variety of substrates. *Int. J. Mol. Sci.* **2024**, *25* (6), 3445.

(15) Silva, G. M. C.; Morgado, P.; Lourenço, P.; Goldmann, M.; Filipe, E. J. M. Spontaneous self-assembly and structure of perfluoroalkylalkane surfactant hemimicelles by molecular dynamics simulations. *Proc. Natl. Acad. Sci. U. S. A.* **2019**, *116* (30), 14868-14873. DOI: 10.1073/pnas.1906782116.

(16) Hollingsworth, S. A.; Dror, R. O. Molecular dynamics simulation for all. *Neuron* **2018**, *99* (6), 1129-1143. DOI: 10.1016/j.neuron.2018.08.011.

(17) Kmiecik, S.; Gront, D.; Kolinski, M.; Wieteska, L.; Dawid, A. E.; Kolinski, A. Coarse-grained protein models and their applications. *Chem. Rev.* **2016**, *116* (14), 7898-7936. DOI: 10.1021/acs.chemrev.6b00163.

(18) Kuo, A.-T.; Urata, S.; Nakabayashi, K.; Watabe, H.; Honmura, S. Coarse-grained molecular dynamics simulation of perfluorosulfonic acid polymer in water–ethanol mixtures. *Macromolecules* **2021**, *54* (2), 609-620. DOI: 10.1021/acs.macromol.0c02364.

(19) Souza, P. C. T.; Alessandri, R.; Barnoud, J.; Thallmair, S.; Faustino, I.; Grünewald, F.; Patmanidis, I.; Abdizadeh, H.; Bruininks, B. M. H.; Wassenaar, T. A. et al. Martini 3: A general purpose force field for coarse-grained molecular dynamics. *Nat. Methods* **2021**, *18* (4), 382-388. DOI: 10.1038/s41592-021-01098-3.

(20) Alessandri, R.; Barnoud, J.; Gertsen, A. S.; Patmanidis, I.; de Vries, A. H.; Souza, P. C. T.; Marrink, S. J. Martini 3 coarse-grained force field: Small molecules. *Adv. Theory Simul.* **2022**, *5* (1), 2100391. DOI: 10.1002/adts.202100391.

(21) U. S., EPA. Designation of perfluorooctanoic acid (PFOA) and perfluorooctanesulfonic acid (PFOS) as cercla hazardous substances. **2024**. https://www.epa.gov/superfund/designation-perfluorooctanoic-acid-pfoa-and-perfluorooctanesulfonic-acid-pfos-cercla (accessed November 1, 2024).

(22) Mejia-Avendaño, S.; Zhi, Y.; Yan, B.; Liu, J. Sorption of polyfluoroalkyl surfactants on surface soils: Effect of molecular structures, soil properties, and solution chemistry. *Environ. Sci. Technol.* **2020**, *54* (3), 1513-1521. DOI: 10.1021/acs.est.9b04989.

(23) Barriet, D.; Lee, T. R. Fluorinated self-assembled monolayers: Composition, structure and interfacial properties. *Curr. Opin. Colloid Interface Sci.* **2003**, *8* (3), 236-242. DOI: 10.1016/S1359-0294(03)00054-2.

(24) Abraham, M. J.; Murtola, T.; Schulz, R.; Páll, S.; Smith, J. C.; Hess, B.; Lindahl, E. GROMACS: High performance molecular simulations through multi-level parallelism from laptops to supercomputers. *SoftwareX* **2015**, *1-2*, 19-25. DOI: 10.1016/j.softx.2015.06.001.

(25) Van Der Spoel, D.; Lindahl, E.; Hess, B.; Groenhof, G.; Mark, A. E.; Berendsen, H. J. C. GROMACS: Fast, flexible, and free. *J. Comput. Chem.* **2005**, *26* (16), 1701-1718. DOI: 10.1002/jcc.20291.

(26) Guan, D.-X.; Li, Y.-Q.; Yu, N.-Y.; Yu, G.-H.; Wei, S.; Zhang, H.; Davison, W.; Cui, X.-Y.; Ma, L. Q.; Luo, J. In situ measurement of perfluoroalkyl substances in aquatic systems using diffusive gradients in thin-films technique. *Water Res.* **2018**, *144*, 162-171. DOI: https://doi.org/10.1016/j.watres.2018.07.031.

(27) Marrink, S. J.; Mark, A. E. Molecular dynamics simulation of the formation, structure, and dynamics of small phospholipid vesicles. *J. Am. Chem. Soc.* **2003**, *125* (49), 15233-15242. DOI: 10.1021/ja0352092.

(28) Krafft, M.-P.; Giuleiri, F.; Riess, J. G. Can single-chain perfluoroalkylated amphiphiles alone form vesicles and other organized supramolecular systems? *Angew. Chem., Int. Ed. Engl.* **1993**, *32* (5), 741-743. DOI: https://doi.org/10.1002/anie.199307411.

(29) Yu, X.; Li, F.; Fang, H.; Miao, X.; Wang, J.; Zong, R.; Lu, S. Foaming behavior of fluorocarbon surfactant used in fire-fighting: The importance of viscosity and self-assembly structure. *J. Mol. Liq.* **2021**, *327*, 114811. DOI: https://doi.org/10.1016/j.molliq.2020.114811.

(30) López-Fontán, J. L.; Sarmiento, F.; Schulz, P. C. The aggregation of sodium perfluorooctanoate in water. *Colloid Polym. Sci.* **2005**, *283* (8), 862-871. DOI: 10.1007/s00396-004-1228-7.

(31) Klevan, C.; Caines, S.; Gomes, A.; Pennell, K. D. Accurate determination of perfluorooctanoate aqueous solubility, critical micelle concentration, and acid dissociation constant. *Environ. Sci. Technol. Lett.* **2024**, *11* (12), 1398-1405. DOI: 10.1021/acs.estlett.4c00858.

(32) Pajtinka, P.; Vácha, R. Amphipathic helices can sense both positive and negative curvatures of lipid membranes. *J. Phys. Chem. Lett.* **2024**, *15* (1), 175-179. DOI: 10.1021/acs.jpclett.3c02785.

(33) Szule, J. A.; Fuller, N. L.; Peter Rand, R. The effects of acyl chain length and saturation of diacylglycerols and phosphatidylcholines on membrane monolayer curvature. *Biophys. J.* **2002**, *83* (2), 977-984. DOI: https://doi.org/10.1016/S0006-3495(02)75223-5.

(34) Kamal, M. M.; Mills, D.; Grzybek, M.; Howard, J. Measurement of the membrane curvature preference of phospholipids reveals only weak coupling between lipid shape and leaflet curvature. *Proc. Natl. Acad. Sci. U. S. A.* **2009**, *106* (52), 22245-22250. DOI: doi:10.1073/pnas.0907354106.

(35) Zaggia, A.; Conte, L.; Falletti, L.; Fant, M.; Chiorboli, A. Use of strong anion exchange resins for the removal of perfluoroalkylated substances from contaminated drinking water in batch and continuous pilot plants. *Water Res.* **2016**, *91*, 137-146. DOI: https://doi.org/10.1016/j.watres.2015.12.039.